Resonant magneto-optic Kerr effect in CdTe/$Cd_{1-x}Mn_xTe$ quantum-well structures

C. Testelin and C. Rigaux
Groupe de Physique des Solides, Universités Paris 6 et 7, 2, place Jussieu, 75231 Paris Cedex 05, France

J. Cibert
Laboratoire de Spectrométrie Physique, Université Joseph Fourier, Grenoble I, Boîte Postale 87, 38402 Saint-Martin d'Hères, France
(Received 21 March 1996; revised manuscript received 9 September 1996)

We present a study of the magneto-optic Kerr effect (MOKE) in the region of the heavy-hole exciton ground state performed on asymmetric quantum wells $Cd_{1-x}Zn_xTe$/CdTe/$Cd_{1-x}Mn_xTe$. A multilayer model developed for quantum-well structures accounts quantitatively for the MOKE line shapes using parameters deduced from magnetoreflectance analysis. The field behavior of energies and intensities of the Kerr resonances underline the interest of MOKE measurements, particularly at low field, where a linear dependence between Zeeman splitting and Kerr angle amplitude has been observed. Comparison is given with calculated Faraday rotation. [S0163-1829(97)02904-4]

I. INTRODUCTION

Heterostructures incorporating diluted magnetic semiconductors (DMS's) display strong magnetooptical effects which originate from ion-carrier exchange interactions in the magnetic layers. In structures made of a nonmagnetic quantum well (QW) surrounded by semimagnetic barriers, such as CdTe/$Cd_{1-x}Mn_xTe$ structures, the magnetic tuning of the barrier potential induces large changes of the confinement energies which appear as large Zeeman effects of the excitons confined in the quantum well.[1–3] A strong magnetic-field dependence of the exciton oscillator strength has been observed in CdTe/$Cd_{0.9}Mn_{0.1}Te$ heterostructures.[4] A consequence of the exciton Zeeman splitting is the strong resonant Faraday rotation which has been observed in CdTe/$Cd_{1-x}Mn_xTe$ multiple quantum wells and superlattices.[5,6] In Ref. 6, the Faraday rotation was directly related to the magnetotransmission spectra using a phenomenological description of the exciton.

Similarly to the Faraday rotation, the magnetooptic Kerr effect (MOKE) originates from the magnetic circular birefringence induced by the Zeeman effect. Preliminary measurements reported for CdTe/$Cd_{1-x}Mn_xTe$ superlattices show the interest of the MOKE to study diluted magnetic semiconductor heterostructures grown on opaque substrates.[7,8]

Reflectance on semiconductor heterostructures was first studied on III–V superlattices[9,10] and more recently on II-VI structures, in the presence of a magnetic field.[4,11] In this paper, we present a detailed study of both the reflectance and the polar MOKE in a static magnetic field performed on CdTe/$Cd_{1-x}Mn_xTe$ single-quantum-well (SQW) structures in the region of the E_1H_1 exciton transition. MOKE spectra obtained at fixed magnetic fields, at $T=1.7$ K, are analyzed within a model of dielectric response developed for single-quantum-well structures. This model quantitatively explains experimental MOKE spectra for exciton parameters deduced from the magnetoreflectance analysis. The present data emphasize the large resonant Kerr rotation found in SQW which, according to our model, reaches a magnitude comparable to that predicted for the resonant Faraday rotation. The Kerr rotation exhibits particularly interesting features at very low field, where the Kerr angle amplitude is proportional to the E_1H_1 exciton Zeeman splitting. In this linear regime, MOKE experiments should provide an access to Mn ions magnetic properties in the barrier layers.

II. EXPERIMENTS

The samples used in this study are two asymmetric $Cd_{1-x}Mn_xTe$/CdTe/$Cd_{1-y}Zn_yTe$ quantum wells grown by molecular-beam epitaxy on (001) $Cd_{0.88}Zn_{0.12}Te$ substrates. These structures belong to a series of samples which have been grown by the CNRS-CEA (Centre National de la Recherche Scientifique–Commissariat à l'Energic Atomique) group of Grenoble to study interface profiles.[2,3] The investigated samples, labeled $M336$ and $M340$ in Ref. 2 ($I2$ and $N2$, respectively, in Ref. 3), contain a CdTe quantum well with two different barriers: one magnetic ($Cd_{1-x}Mn_xTe$) and one nonmagnetic ($Cd_{1-y}Zn_yTe$). The essential difference between the two samples is the growth direction: in sample M340, the magnetic barrier was grown after the CdTe quantum well, while in sample M336 the growth order is opposite. The growth procedure and the characteristics of both structures are given in Refs. 2 and 3, where Zeeman splittings are reported. Layers have been grown on a substrate and a buffer $Cd_{1-z}Zn_zTe$ ($z=0.11$–0.12). Sample $M336$ contains four layers whose composition and thicknesses are, along the growth axis, $Cd_{1-x}Mn_xTe$ (19.4 Å)/CdTe (43.2 Å)/$Cd_{1-y}Zn_yTe$ (75.5 Å)/$Cd_{1-x}Mn_xTe$ (220 Å), with $x=0.351$ and $y=0.112$. Sample $M340$ contains five layers: $Cd_{1-x}Mn_xTe$ (230 Å)/$Cd_{1-y}Zn_yTe$ (76.5 Å)/CdTe (46.7 Å)/$Cd_{1-x}Mn_xTe$ (19.4 Å)/$Cd_{1-y}Zn_yTe$ (460 Å), with $x=0.32$ and $y=0.117$.

We have performed magnetooptical experiments, at $T=1.7$ K, in the Faraday geometry, i.e., with magnetic field applied perpendicularly to the layer plane ($H//z$). Magnetoreflectance measurements were made at near-normal incidence with circularly polarized radiation. Polar MOKE experiments were carried out using a method very similar to that described by Sato.[12] A monochromatic radiation obtained from a tunable grating source is linearly polarized at 45° of the axes (x,y) of a photobirefringent modulator. A time periodic retardation $\delta=\delta_0 \sin(2\pi ft)$ is introduced between the orthogonal components (x,y) at the frequency $f=50$ kHz. After near-normal reflection on the sample, the component x (or y), selected by the analyzer, is detected by the photomultiplier. The output signal of the detector consists of a dc component which is proportional to the reflected light intensity I_0R, and ac components at the harmonics of the frequency f. The $2f$ component is proportional to $I_0R \sin 2\theta_K$, where θ_K is the Kerr rotation. A feedback of the dc signal to the photomultiplier high-voltage supply insures a constant value of I_0R in the investigated spectral range. The signal at the frequency $2f$ detected by a lock-in amplifier provides the relative magnitude of $\sin 2\theta_K$. Absolute values of the Kerr rotation angle are obtained by calibration of the $2f$ signal obtained by a small rotation of the analyzer in the absence of magnetic field.

III. MODEL

Magneto-optic Kerr effect

Similarly to the Faraday rotation, the MOKE results from the magnetic circular birefringence of the medium. Linearly polarized radiation propagating along the magnetic-field direction $(H//z)$ becomes elliptically polarized in the (x,y) plane after reflection on the sample surface. The angle of the major axis with the incident polarization direction defines the Kerr rotation θ_K, which is given by

$$\theta_K=\frac{1}{2}\arg\frac{r^-}{r^+}, \tag{1}$$

in terms of the complex amplitude reflection coefficients $r^\pm$ associated with the $\sigma^\pm$ circular eigenmodes propagating in the medium.

The theoretical dependence $\theta_K(\omega)$ is determined by expressing the reflection coefficients $r^\pm$ in terms of the frequency-dependent dielectric function $\varepsilon_\pm=\varepsilon_{xx}\mp i\varepsilon_{xy}$ associated with each $\sigma^\pm$ eigenmode. For a normal reflection on a bulk material, the coefficients $r^\pm$ are

$$r^\pm=\frac{1-\sqrt{\varepsilon_\pm}}{1+\sqrt{\varepsilon_\pm}}, \tag{2}$$

ε_{xx} and ε_{xy} denote the diagonal and off-diagonal elements of the dielectric tensor of the cubic crystal in the magnetic field.[19]

For a multilayer structure, the coefficients $r^\pm$ depend on the amplitude reflection coefficients $r^\pm_{i,i+1}$ at the interfaces of successive layers i. If we approximate a single quantum well by a three-layer structure, in the case of normal reflection, $r^\pm$ takes the form

$$r^\pm=\frac{r^\pm_{01}+r^\pm_{123}e^{2i\beta_1^\pm}}{1+r^\pm_{01}\;r^\pm_{123}e^{2i\beta_1^\pm}}, \tag{3}$$

where

$$r^\pm_{123}=\frac{r^\pm_{12}+r^\pm_{23}e^{2i\beta_2^\pm}}{1+r^\pm_{12}\;r^\pm_{23}e^{2i\beta_2^\pm}}. \tag{4}$$

The reflection coefficient $r^\pm_{i,i+1}(i\geqslant 0)$, at the interface $(i,\, i+1)$, is related to the dielectric function $\varepsilon_i^\pm$ of the adjacent layers by

$$r^\pm_{i,i+1}=\frac{\sqrt{\varepsilon_i^\pm}-\sqrt{\varepsilon_{i+1}^\pm}}{\sqrt{\varepsilon_i^\pm}+\sqrt{\varepsilon_{i+1}^\pm}}. \tag{5}$$

$\beta_i^\pm=(\omega/c)\, l_i\sqrt{\varepsilon_i^\pm}$ denotes the dephazing of the electric field radiation after crossing the layer i of thickness l_i.

Expressions (3) and (4) of the reflection coefficients can be easily generalized to multilayer structures with more than three layers.

Dielectric function in a quantum well

Different approaches can be used to determine the frequency-dependent dielectric function near the exciton resonance frequency. In the Appendix, we treat the QW as a homogeneous medium, and we derive $\varepsilon_\pm(\omega)$ from the mean value of the dielectric polarization calculated from time-dependent perturbation theory. This treatment leads to Eq. (A8).

A more rigorous method based on the nonlocal susceptibility calculated within the linear-response theory can be applied to derive $\varepsilon_\pm(\omega,z)$ along the z axis. This procedure was previously developed by Ivchenko[13] and Ivchenko *et al.*[4] to determine the reflection and transmission coefficients of an isolated QW enclosed between semi-infinite barriers. The electric field $\vec{E}(z)$ and the local dielectric function $\varepsilon_\pm(z,\omega)$ satisfy the equation

$$\varepsilon_\pm(z,\omega)\vec{E}(z)=\varepsilon_1\vec{E}(z)\;+\;4\pi\vec{P}_\pm(z), \tag{6}$$

where $\vec{P}_\pm$ is the contribution of the exciton resonance (at frequency $\omega_\pm$) to the electric polarization, and ε_1 is the background dielectric constant, including the contribution of all nonresonant states.

The linear-response theory yields[14,15]

$$\vec{P}_\pm(z)=\int \chi_\pm(z,z')\vec{E}(z')\;dz'. \tag{7}$$

The generalized susceptibility $\chi_\pm(z,z')$ is given as

$$\chi_\pm(z,z')=\frac{e^2P^2_{\rm cv}}{\hbar m^2\omega^2_\pm}\;\frac{\phi_\pm(z)\;\;\phi_\pm(z')}{\omega_\pm-\omega-i\Gamma_\pm}=\beta_\pm\phi_\pm(z)\phi_\pm(z'), \tag{8}$$

where $\Gamma_\pm$ is the nonradiative damping term. $\phi_\pm(z)=F_\pm(0)\varphi^c_\pm(z)\varphi^v_\pm(z)$. $F_\pm(\vec{r})$ is the exciton envelope function; $\varphi^c_\pm$ and $\varphi^v_\pm$ are the envelope functions of electron and hole confined states, defined in the Appendix; and $P_{\rm cv}$ is the matrix element of the momentum operator between the conduction and valence states.

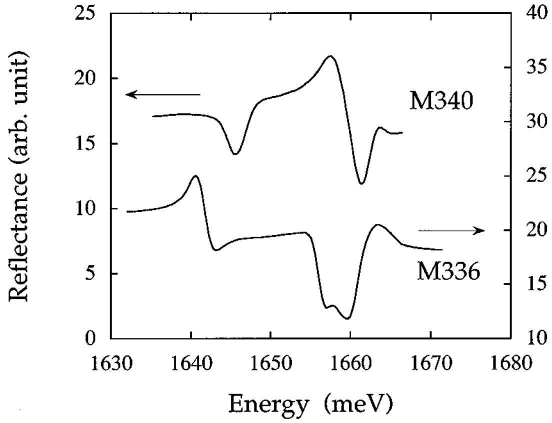

FIG. 1. Zero field reflectivity spectra, at $T=1.7$ K of samples $M336$ and $M340$.

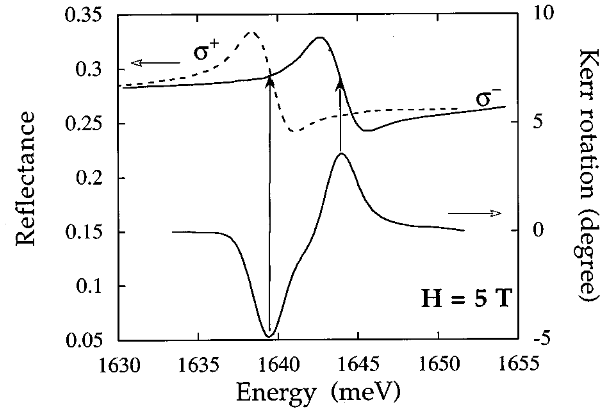

FIG. 2. Comparison between Kerr rotation (lower curve) and magnetoreflectance spectra (upper curves) measured at $T=1.7$ K for $H=5$ T on sample $M336$, in the region of the E_1H_1 exciton.

By solving the differential wave equation[13] for an incident circular plane wave $\vec{E}_\pm(z)=\vec{E}^0_\pm e^{ikz}=E^0(\vec{x}\mp i\vec{y})e^{ikz}$, one obtains

$$\vec{E}_\pm(z)=\vec{E}^0_\pm e^{ikz}+2\pi i\frac{k}{\varepsilon_1}\int \vec{P}_\pm(z')e^{ik|z-z'|}\,dz', \tag{9}$$

with $k=\sqrt{\varepsilon_1}\omega/c$.

Solving Eqs. (6) and (9) by iteration, one obtains a general expression for $\varepsilon_\pm(z,\omega)$:

$$\varepsilon_\pm(z,\omega)=\varepsilon_1+\frac{4\pi\mu^k_\pm\beta_\pm\phi_\pm(z)e^{-ikz}}{1-\dfrac{i\omega}{c\sqrt{\varepsilon_1}}2\pi\beta_\pm(\theta^k_\pm-f^k_\pm(z)\mu^k_\pm e^{-ikz})}, \tag{10}$$

with the condition of convergence of the iteration:

$$\left|\frac{2\pi\beta_\pm k}{\varepsilon_1}\theta^k_\pm\right|<1. \tag{11}$$

We will come back to this condition later on. $\mu^k_\pm$, $f^k_\pm$, and $\theta^k_\pm$ are defined by

$$\mu^k_\pm=\int \phi_\pm(z)e^{ikz}\,dz,$$

$$f^k_\pm(z)=\int \phi_\pm(z')e^{ik|z-z'|}\,dz',$$

$$\theta^k_\pm=\int \theta_\pm(z)f^k_\pm(z)\,dz. \tag{12}$$

In the limit $kL/2\ll 1$ [i.e., for $L/\lambda\ll 1/\pi\sqrt{\varepsilon_1}$; λ is the wavelength of the incident light, in vacuum), Eq. (10) takes the simplified form

$$\varepsilon_\pm(z,\omega)=\varepsilon_1+\frac{4\pi e^2P^2_{cv}}{\hbar m^2\omega^2_\pm}\,\frac{\phi_\pm(z)\left(\int \phi_\pm(z')\,dz'\right)}{\omega_\pm-\omega-i\Gamma_\pm}. \tag{13}$$

The average value $(1/L)\int_{\rm well}\varepsilon_\pm(z,\omega)\,dz$ in the QW is identical to the value $\varepsilon_\pm(\omega)$ derived in the Appendix.

In the present study, the approximation $kL/2\ll 1$ is reasonably satisfied, and we will use the theoretical expression (A8) of the dielectric function in a magnetic field, for the quantitative analysis of magnetoreflectance and MOKE spectra in the vicinity of the QW exciton ground state.

An alternative analysis will be also performed by using the expression of the reflection coefficient of a SQW calculated from the nonlocal dielectric response theory.[4] For a normally incident circular radiation propagating along the z axis, the reflection coefficient $r^\pm_{123}$ of a QW enclosed between semiinfinite barriers is[14]

$$r^\pm_{123}=\frac{i\tilde{\Gamma}_\pm}{\tilde{\omega}_\pm-\omega-i(\Gamma_\pm+\tilde{\Gamma}_\pm)}. \tag{14}$$

In the limit kL/2≪1,

$$\tilde{\omega}_\pm=\omega_\pm$$

and

$$\tilde{\Gamma}_\pm=\frac{2\pi e^2P^2_{cv}}{\hbar m^2\omega^2_\pm}\,\frac{k}{\varepsilon_1}\left(\int \phi_\pm(z)\,dz\right)^2=\pi\sqrt{\varepsilon_1}\,\frac{L}{\lambda}\,\gamma_\pm. \tag{15}$$

With these notations, one writes the condition of convergence, Eq. (11), $\tilde{\Gamma}_\pm<\Gamma_\pm$.

We will show in Sec. IV that the analysis of the experimental spectra performed by using the frequency-dependent dielectric function [Eq. (A8)] or the reflection coefficient [Eq. (14)] are equivalent and lead to coherent values of parameters which satisfy the relation $\tilde{\Gamma}_\pm<\Gamma_\pm$.

IV. RESULTS AND DISCUSSION

Zero-field reflectivity spectra obtained at T = 1.7 K in the spectral region ($1630\leq\hbar\omega\leq 1670$ meV) are reported in Fig. 1. The low-energy structure at $\hbar\omega_0=1641.9$ meV ($M336$) and 1645.3 meV ($M340$) corresponds to the quantum well heavy-hole exciton, while the features at 1656–1660 meV are attributed to the excitons in $Cd_{1-y}Zn_yTe$ substrates and buffer layers whose Zn composition is slightly different (cf. Sec. II). These latter are nearly independent of magnetic field, while the structure at $\hbar\omega_0$ exhibits Zeeman

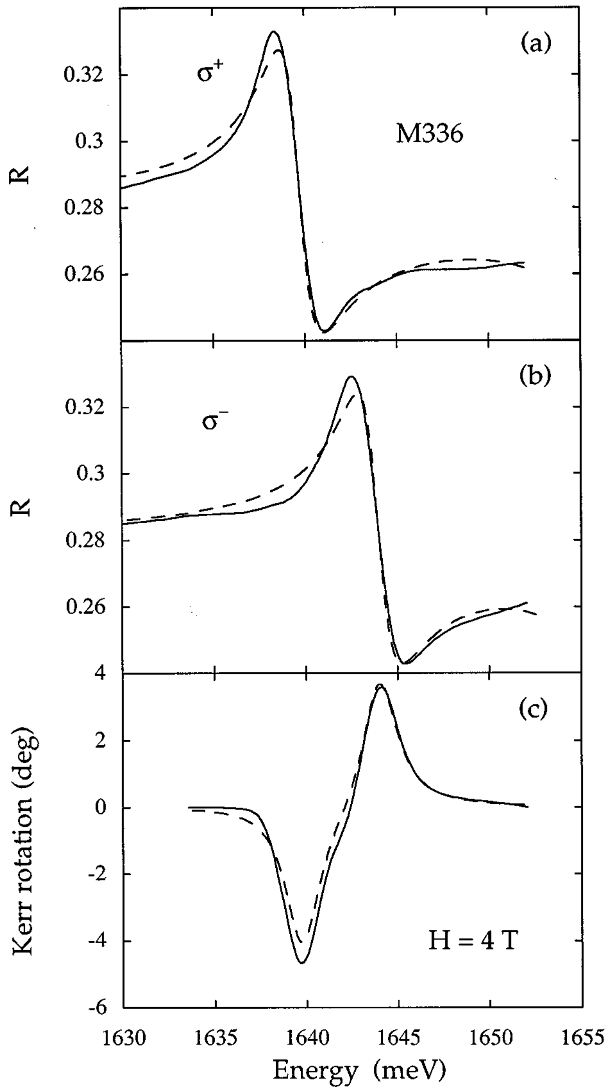

FIG. 3. Magnetoreflectance and MOKE spectra in the region of the QW E_1H_1 exciton for sample $M336$, $T=1.7$ K and $H=4$ T. Solid lines are experimental data. Dashed lines in (a) and (b) are the best theoretical fits of $R^{\pm}=|r^{\pm}|^2$ calculated from the multilayer model for the parameters $\hbar\gamma^{+}=0.82$ meV, $\hbar\Gamma^{+}=1.03$ meV, $\hbar\omega_0^{+}=1639.6$ meV, $\hbar\gamma^{-}=0.8$ meV, $\hbar\Gamma^{-}=1.05$ meV, and $\hbar\omega_0^{-}=1643.8$ meV. The dashed line in (c) represents the Kerr rotation θ_K calculated from Eqs. (1) and (4)–(6) for the above values of parameters.

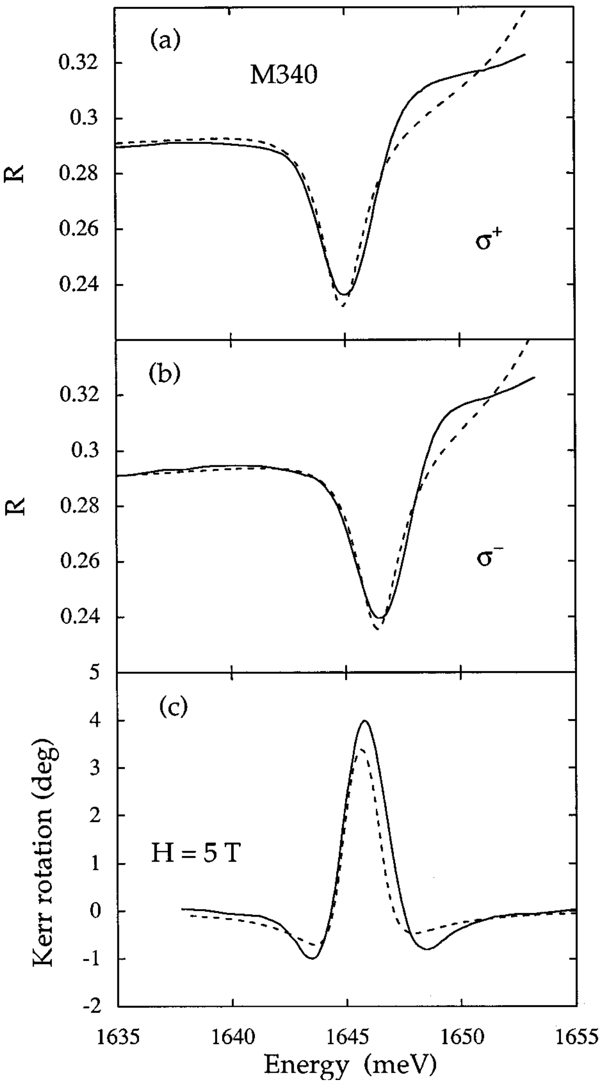

FIG. 4. The same as in Fig. 3, for sample $M340$, at $H=5$ T. $\hbar\gamma^{+}=0.67$ meV, $\hbar\Gamma^{+}=1.09$ meV, $\hbar\omega_0^{+}=1644.8$ meV, $\hbar\gamma^{-}=0.68$ meV, $\hbar\Gamma^{-}=1.12$ meV, and $\hbar\omega_0^{-}=1646.3$ meV.

splittings, shown in Figs. 3 and 4.

The comparison between MOKE and magnetoreflectance spectra is illustrated in Fig. 2 for sample $M336$, at $H=5$ T. The Kerr rotation exhibits two peaks of opposite sign which occur near the inflection points of the magnetoreflectivity structures: the negative (positive) peak of θ_K corresponds to the σ^{+} (σ^{-}) Zeeman components of the reflectivity.

Magnetoreflectance ($\sigma^{\pm}$) and MOKE spectra were measured in the region of the QW exciton ($1630\leqslant\hbar\omega\leqslant1655$ meV) for different fields ($H\leqslant5$ T) parallel to the growth axis. The data are reported in Figs. 3 and 4 for both investigated samples. The line shape of the $\sigma^{\pm}$ magnetoreflectance spectra is analyzed in the framework of the model developed for a multilayer structure. The comparison between calculated and experimental reflectance spectra yields the QW exciton parameters. MOKE spectra are then calculated for these parameters, and compared with the experimental data.

Each sample is considered as a multilayer structure according to the description given in Sec. II. The reflectance coefficient $R^{\pm}=|r^{\pm}|^2$ of each heterostructure is determined from Eqs. (3)–(5) in terms of the reflection coefficients $r^{\pm}_{i,i+1}$ which depend on the dielectric function associated with each layer $\varepsilon_i^{\pm}$. In the region of the QW exciton ground state, the frequency-dependent dielectric function $\varepsilon_{\pm}(\omega)$ for the asymmetric quantum well follows Eq. (A8).

In the investigated energy range, the dielectric constant ε_b in the $Cd_{1-x}Mn_xTe$ barriers is frequency independent. Since the exciton energy $\hbar\omega_{Zn}$ in $Cd_{1-y}Zn_yTe$ thick layers differs from $\hbar\omega_{\pm}$ by about 10–15 meV, we use a frequency-dependent dielectric function $\varepsilon_{Zn}(\omega)$ for the $Cd_{1-y}Zn_yTe$ thick layers:

$$\varepsilon_{\mathrm{Zn}}(\omega)=\varepsilon_1'\left[1+\frac{\gamma_{\mathrm{Zn}}}{\omega_{\mathrm{Zn}}-\omega-i\Gamma_{\mathrm{Zn}}}\right], \tag{16}$$

with parameters (ω_{Zn}, γ_{Zn}, Γ_{Zn}) independent of magnetic field.

For the sake of simplicity, we assume identical background dielectric constants for the quantum well and for $Cd_{1-y}Zn_yTe$ or $Cd_{1-x}Mn_xTe$ layers [$\varepsilon_1=\varepsilon_1'=\varepsilon_b=10.6$ (Ref. 16)]. We also assume identical compositions for all $Cd_{1-y}Zn_yTe$ layers in the same sample.

The reflectance coefficient $R^{\pm}(\omega)$ is calculated within the multilayer model taking the layer thickness l_i as indicated in Sec. II. Since carriers are confined in both CdTe and $Cd_{1-y}Zn_yTe$ layers of the asymmetric quantum well,[3] we take them as a whole ''QW layer'' with an effective QW width $L=l_{\mathrm{CdTe}}+l_{\mathrm{Cd}_{1-y}\mathrm{Zn}_y\mathrm{Te}}$.

First, the parameters ($\hbar\omega_{\mathrm{Zn}}$, $\hbar\gamma_{\mathrm{Zn}}$, $\hbar\Gamma_{\mathrm{Zn}}$) of $\varepsilon_{\mathrm{Zn}}(\omega)$ are estimated from the fit of the exciton reflectivity structure in the $Cd_{1-y}Zn_yTe$ buffer and substrate layers. For $M336$, we kept only the low energy $Cd_{1-y}Zn_yTe$ structure. We obtained the following parameters for both samples:

$$\hbar\omega_{\mathrm{Zn}}'=1657\text{–}1658\ \mathrm{meV},\quad \hbar\gamma_{\mathrm{Zn}}=0.6\text{–}0.7\ \mathrm{meV},$$

$$\hbar\Gamma_{\mathrm{Zn}}=1\text{–}1.2\ \ \mathrm{meV}. \tag{17}$$

Second, the reflectance coefficient $R^{\pm}(\omega)$, associated with the $\sigma^{\pm}$ polarization, is calculated for different magnetic fields, taking the above values (17) of the parameters. The QW exciton parameters ($\hbar\omega_{\pm}$, $\hbar\gamma_{\pm}$, $\hbar\hat{\Gamma}_{\pm}$) are then determined from the best agreement between theoretical and experimental spectra in the region of the QW E_1H_1 exciton. At zero field, the best fit of $R(\omega)$ corresponds to the following values of the parameters:

$$M336\begin{cases}\hbar\omega_0=1641.9\ \ \mathrm{meV}\\ \hbar\gamma=0.83\ \ \mathrm{meV}\\ \hbar\Gamma=1.05\ \ \mathrm{meV},\end{cases}$$

$$M340\begin{cases}\hbar\omega_0=1645.3\ \ \mathrm{meV}\\ \hbar\gamma=0.6\ \ \mathrm{meV}\\ \hbar\Gamma=1.05\ \ \mathrm{meV}.\end{cases} \tag{18}$$

It is useful to compare these parameters with the radiative and nonradiative linewidths ($\tilde{\Gamma}$ and Γ, respectively) obtained from the analysis of the reflectivity spectra performed by using the expression (14) of the reflection coefficient r_{123} derived within the nonlocal dielectric theory in the limit $kL/2\ll 1$. This approximation is well justified in the case of the samples $M336$ and $M340$, of QW widths $L=119$–120 Å. The condition $\tilde{\Gamma}_{\pm}<\Gamma_{\pm}$ is also verified for these samples. The best fits of the reflectivity structures in both samples are achieved for the parameters

$$M336\begin{cases}\hbar\omega_0=1641.9\ \ \mathrm{meV}\\ \hbar\tilde{\Gamma}=0.13\ \ \mathrm{meV}\\ \hbar\Gamma=1.05\ \ \mathrm{meV},\end{cases}$$

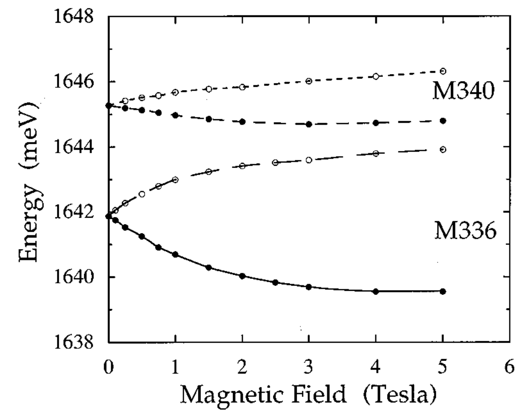

FIG. 5. Energies of the Zeeman components vs magnetic field (●, σ^+; ○, σ^-). Lower curves: sample $M336$; upper curves: $M340$.

$$M340\begin{cases}\hbar\omega_0=1645.4\ \ \mathrm{meV}\\ \hbar\tilde{\Gamma}=0.09\ \ \mathrm{meV}\\ \hbar\Gamma=1\ \ \mathrm{meV}.\end{cases} \tag{19}$$

These values of parameters ($\tilde{\Gamma}$, Γ, ω_0) are coherent with parameters (γ,Γ,ω_0) deduced from our previous analysis (18), the ratio between the radiative linewidth $\tilde{\Gamma}$ and the parameter γ satisfying the relation (15). The radiative linewidth $\tilde{\Gamma}$ obtained for samples $M336$ and $M340$ are comparable to the values given in Refs. 4 and 17 for single or multiple quantum wells.

The fits of magnetoreflectance line shape $R^{\pm}(\omega)$ yield the energies $\hbar\omega_{\pm}$ of the QW exciton Zeeman components which are reported in Fig. 5 versus magnetic field, for both samples. The damping term $\Gamma_{\pm}$ and the parameter $\gamma_{\pm}$ obtained from the fitting procedure do not depend significantly on magnetic field. Moreover, comparable values are found for $\sigma^{\pm}$ polarization. In the investigated field range, we obtain $\hbar\gamma_{\pm}=0.83\pm0.03$ meV and $\hbar\Gamma_{\pm}=1.07\pm0.04$ meV for $M336$; $\hbar\gamma_{\pm}=0.64\pm0.04$ meV and $\hbar\Gamma_{\pm}=1.09\pm0.04$ meV for $M340$. Calculated and experimental magnetoreflectance spectra are presented in Figs. 3 and 4. The model accounts quantitatively for the experimental reflectance $R^{\pm}(\omega)$ and for the different line shape observed in both samples: $R^{\pm}(\omega)$ has a steplike structure (similarly as in the bulk) for $M336$ (Figs. 3) while a resonant peak is found in $M340$ (Figs. 4). The line shape depends on the thickness of the cladding layer where multiple interferences occur.

Third, using the above QW exciton parameters and the layer thicknesses reported in Sec. II, the Kerr rotation $\theta_K(\omega)$ is calculated numerically from Eqs. (1) and (3)–(5) in the region of the QW E_1H_1 exciton transition. Figures 3–4(c) show the comparison between the theoretical dependence $\theta_K(\omega)$ and the experimental spectra. *Without an adjustable parameter*, the theoretical model reproduces quite well the experimental spectra of the Kerr effect at different fields, for both structures. This model accounts for a sample-dependent line shape: the Kerr rotation presents two peaks of opposite sign (as in sample $M336$) or a strong maximum surrounded by two weak minima ($M340$). The multilayer model explains quantitatively this difference in the line

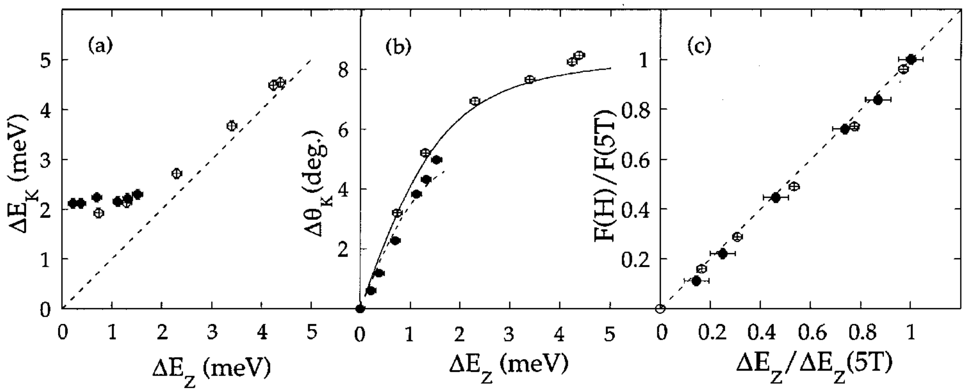

FIG. 6. (a) Energy distance ΔE_K between the extrema of the Kerr rotation as a function of the Zeeman splitting $\Delta E_Z = \hbar\omega_0^- - \hbar\omega_0^+$. The dashed line corresponds to $\Delta E_K = \Delta E_Z$. (b) Amplitude of the Kerr rotation $\Delta\theta_K = \theta_{\max} - 0_{\min}$ as a function of the Zeeman splitting $\Delta E_Z = \hbar\omega_0^- - \hbar\omega_0^+$ at $T = 1.7$ K. Solid and dashed lines are calculated from the model, for samples M336 and M340, respectively. (c) Product $F(H) = \Delta\theta_K \Delta E_K$ vs Zeeman splitting ΔE_Z. Both quantities are normalized by their value at $H = 5$ T. Open and closed symbols are experimental results for samples M336 and M340, respectively.

shape which is related to the thickness d of the cap layer. According to our model, the maximum of the MOKE signal at the resonance is obtained for constructive interferences in the cladding layer, i.e., for a thickness d satisfying $2\sqrt{\varepsilon_1}d = p(\lambda/2)$ (p integer). This condition is approximately verified for sample M340.

It is interesting to compare the energy splitting ΔE_K of the Kerr resonances with the Zeeman splitting ΔE_Z. Figure 6(a) shows the energy distance ΔE_K between the positive and negative peaks, measured on sample M336, as a function of $\Delta E_Z = \hbar\omega_0^- - \hbar\omega_0^+$. In the field range where ΔE_K exceeds 2Γ, the separation of the Kerr components is comparable to the Zeeman splitting, while ΔE_K becomes constant in the low-field region.

The amplitude of the Kerr rotation $\Delta\theta_K = \theta_K^{\max} - \theta_K^{\min}$ measured on the same sample, reported on Fig. 6(b), increases linearly with the Zeeman splitting at low field, and tends to saturate at high field.

For sample M340, which presents a weaker Zeeman splitting (Fig. 5), the energy distance ΔE_K between the extrema is constant, and a linear regime is found in the whole investigated field range [Fig. 6(a)]. The observed behavior of the Kerr splitting ΔE_K and of the amplitude $\Delta\theta_K$ in the low-field region is the manifestation of overlapping Zeeman components in the Kerr spectrum. This situation occurs typically when $\hbar\omega_- - \hbar\omega_+ \leqslant 2\Gamma$. These features are well explained, with the experimental accuracy, by the theoretical variation $\Delta\theta_K$ versus ΔE_Z calculated from the model [Fig. 6(b)] which reproduces quite well the observed dependence.

Another interesting quantity is the product $F(H) = \Delta\theta_K \cdot \Delta E_K$ of the Kerr angle amplitude and the Kerr splitting. This product is reported in Fig. 6(c) as a function of the Zeeman splitting ΔE_Z, for both samples. A linear dependence is observed in the whole investigated field range.

The present study demonstrates the validity of the model to describe magneto-optical properties in QW heterostructures based on DMS's. These DMS heterostructures are usually grown on opaque substrates (GaAs, $Cd_{0.96}Zn_{0.04}Te$, etc.), which prevent Faraday rotation measurements at the resonance of the QW exciton. We have calculated the Faraday rotation in our model for parameters of sample M336. Results are reported in Fig. 7, together with the experimental MOKE spectrum at $H = 1$ T. The amplitude of the Kerr rotation is comparable to that of the Faraday effect, while the resonances have opposite signs in both types of experiments.

In DMS's, the Zeeman splitting is related to the Mn ion magnetization, via ion-carrier exchange; at low field, in the region where $\Delta\theta_K \propto \Delta E_Z$, the MOKE measurements provide optical access to the Mn magnetization in the barrier layers. Thus Kerr rotation experiments could offer interesting possibilities, similarly to the Faraday rotation,[18] to study spin-glass properties and critical dynamics in systems with reduced dimensionality.[7]

ACKNOWLEDGMENT

The authors wish to thank Professor J. A. Gaj for helpful discussions and interesting comments.

APPENDIX

We derive the frequency-dependent dielectric function $\varepsilon_{\pm}(\omega)$ in the region of the exciton ground state for a DMS and for a single quantum-well structure, where the quantum well is approximated by a homogeneous layer of thickness L. The components $\varepsilon_{\alpha\beta}(\omega)$ of the dielectric tensor have already been determined from the mean value of the electric polarization in the framework of the time-dependent perturbation theory.[19] In a magnetic field applied along the light

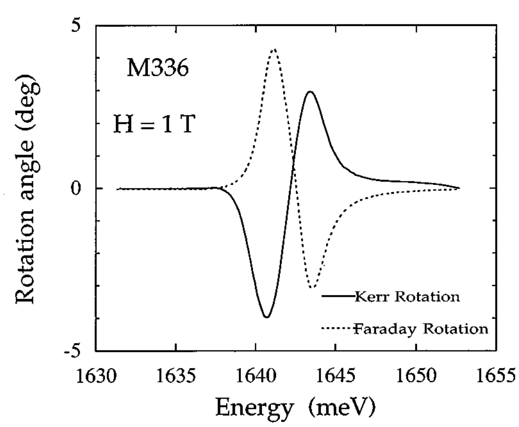

FIG. 7. Comparison between Kerr and Faraday rotations. Solid line: experimental Kerr rotation (sample M336, $T = 1.7$ K, $H = 1$ T). Dashed line: Faraday rotation calculated from the multilayer model for parameters obtained from the fits of $R^{\pm}(\omega)$.

propagation axis ($H//z$), the dielectric function $\varepsilon_{\pm}(\omega)=\varepsilon_{xx}\mp i\varepsilon_{xy}$ is associated with $\sigma^{\pm}$ circular eigenmodes. Dealing with exciton states, it is convenient to express $\varepsilon_{\pm}(\omega)$ in a two-particle formalism[20,21]

$$\varepsilon_{\pm}(\omega)=1-\frac{2\pi e^2}{\hbar\omega m^2}\frac{1}{\Omega}\times\sum_f \frac{1}{\omega_f}\left(\frac{|\langle\psi_f|p_{\mp}|0\rangle|^2}{\omega+\omega_f+i\Gamma_f}+\frac{|\langle\psi_f|p_{\pm}|0\rangle|^2}{\omega-\omega_f+i\Gamma_f}\right), \tag{A1}$$

where $\vec{p}$ is the momentum operator and $p_{\pm}=p_x\pm ip_y\cdot|0\rangle$ is the ground state with all valence states occupied and empty conduction bands. Ω is the volume of the sample, Γ_f is a damping term. The sum runs over excited states f, of wave function ψ_f and energy $\hbar\omega_f$. The states f are excitons built from conduction and valence bands at $\vec{k}_e+\vec{k}_h=\vec{0}$.

We consider now a DMS of zinc-blende structure in a magnetic field $H//z$, with the Γ_6 and Γ_8 bands edges split by the sp-d exchange interaction. Using the effective-mass approximation, the excited states f are excitons of angular momentum $j=\pm 1$, involving both light and heavy holes. The corresponding wave functions are

$$\psi_{\pm}^{\mathrm{hh}}(\vec{r}_e,\vec{r}_h)=\frac{1}{\sqrt{\Omega}}F_{\pm}^{\mathrm{hh}}(\vec{r}_e-\vec{r}_h)u_{\mp 3/2}^{v}(\vec{r}_h)u_{\mp 1/2}^{c}(\vec{r}_e), \tag{A2a}$$

$$\psi_{\pm}^{\mathrm{lh}}(\vec{r}_e,\vec{r}_h)=\frac{1}{\sqrt{\Omega}}F_{\pm}^{\mathrm{lh}}(\vec{r}_e-\vec{r}_h)u_{\mp 1/2}^{v}(\vec{r}_h)u_{\pm 1/2}^{c}(\vec{r}_e), \tag{A2b}$$

where $u_{m_s}^{c}$ are conduction Bloch functions associated with spin states $m_s=\pm 1/2$ and $u_{m_J}^{v}$ denote the valence Bloch functions associated with states of angular momentum component $m_J=\pm 3/2$, $\pm 1/2$. $F_{\pm}$ in Eq. (A2) denotes the exciton envelope function associated with $j=\pm 1$. $\vec{r}_e$ and $\vec{r}_h$ denote the vector position of electron and hole with wave vectors $\vec{k}_e$ and $\vec{k}_h$, respectively.

Using Eqs. (A1) and (A2) and the relation[22]

$$|\langle\psi_f|p_\alpha|0\rangle|^2\cong\Omega|\langle u_c|p_\alpha|u_v\rangle|^2|F_f(0)|^2, \tag{A3}$$

one obtains the expression of $\varepsilon_{\pm}(\omega)$. Near the resonant transition,

$$\varepsilon_{\pm}(\omega)=\varepsilon_1+\frac{4\pi e^2}{\hbar\omega m^2}P^2\left[\frac{1}{\omega_{\mathrm{hh}}^{\pm}}\frac{|F_{\pm}^{\mathrm{hh}}(0)|^2}{\omega_{\mathrm{hh}}^{\pm}-\omega-i\Gamma_{\mathrm{hh}}^{\pm}}+\frac{1}{3\omega_{\mathrm{lh}}^{\pm}}\frac{|F_{\pm}^{\mathrm{lh}}(0)|^2}{\omega_{\mathrm{lh}}^{\pm}-\omega-i\Gamma_{\mathrm{hh}}^{\pm}}\right]. \tag{A4}$$

ε_1 is the background dielectric constant involving both the nonresonant terms in (A1) and the contribution of all allowed transitions. $\hbar\omega_{\mathrm{hh}}^{\pm}$ and $\hbar\omega_{\mathrm{lh}}^{\pm}$ are the energies of the exciton transitions;

$$\hbar\omega_{\mathrm{hh}}^{\pm}=E_0\ \pm\ \frac{1}{2}\ N_0(\alpha-\beta)x\langle S_z\rangle,$$
$$\hbar\omega_{\mathrm{lh}}^{\pm}=E_0\mp\ \frac{1}{2}\ N_0(\alpha+\beta/3)x\langle S_z\rangle, \tag{A5}$$

where E_0 is the zero-field exciton energy; $N_0\alpha$ and $N_0\beta$ are the exchange integrals for Γ_6 and Γ_8 bands, respectively; x is Mn molar fraction; $\langle S_z\rangle$ denotes the mean value of the Mn spin along the magnetic field; $P=\langle S|p_x|x\rangle$ is the $\Gamma_8\rightarrow\Gamma_6$ interband matrix element.

Let us now consider a quantum well of width L and area S with the growth axis parallel to z. The dielectric function $\varepsilon_{\pm}(\omega)$ in the well is derived from the general expression (A1) replacing Ω by LS, and taking into account confinement effects. In a DMS of zinc-blende structure, near the E_1H_1 exciton transition, we consider the heavy-hole exciton confined states[23] $\psi_{\pm}$ of angular momentum $j=\pm 1$, with the wave functions written as

$$\psi_{\pm}(\vec{r}_e,\vec{r}_h)=\frac{1}{\sqrt{S}}F_{\pm}(\vec{r}_{e_\perp}-\vec{r}_{h_\perp})\times u_{\mp 3/2}^{v}(\vec{r}_h)\varphi_{\mp 3/2}^{h}(z_h)\ \ u_{\mp 1/2}^{c}(\vec{r}_e)\ \ \varphi_{\mp 1/2}^{e}(z_e) \tag{A6}$$

in terms of the band-edge Bloch functions and envelope functions $F_{\pm}(\vec{r}_{e_\perp}-\vec{r}_{h_\perp})$ in the layer plane and $\varphi_{\mp 1/2}^{e}(z_e)$, $\varphi_{\mp 3/2}^{h}(z_h)$ in the z direction.

Using Eqs. (A1)–(A3),

$$\varepsilon_{\pm}(\omega)=\varepsilon_1+\frac{4\pi e^2}{\hbar\omega m^2}\frac{P^2}{L}\frac{1}{\omega_{\pm}}\frac{|F_{\pm}(0)|^2}{\omega_{\pm}-\omega-i\Gamma_{\pm}}\times\left|\int_{\mathrm{well}}\varphi_{\mp 3/2}^{h}(z)\ \ \varphi_{\mp 1/2}^{e}(z)dz\right|^2, \tag{A7}$$

ε_1 is the background dielectric constant involving all allowed transitions. $\hbar\omega_{\pm}$ denotes the energies of the E_1H_1 exciton transition allowed for $\sigma^{\pm}$ circular polarization. $\Gamma_{\pm}$ is a damping term.

Due to the evanescence of the envelope functions $\varphi_{\mp 1/2}^{e}(z_e)$ and $\varphi_{\mp 3/2}^{h}(z_h)$ in the barrier, the integral in expression (A7) can be estimated over the whole sample and the contribution of the excited states $\psi_{\pm}$ to the barrier dielectric constant can be reasonably neglected. Finally, $\varepsilon_{\pm}(\omega)$, in the well, can be written

$$\varepsilon_{\pm}(\omega)=\varepsilon_1\left[1+\frac{\gamma_{\pm}}{\omega_{\pm}-\omega-i\Gamma_{\pm}}\right], \tag{A8}$$

with

$$\gamma_{\pm}=\frac{4\pi e^2}{\hbar m^2(\omega_{\pm})^2}\frac{P^2}{\varepsilon_1 L}|F_{\pm}(0)|^2|\langle\varphi_{\mp 3/2}^{h}|\varphi_{\mp 1/2}^{e}\rangle|^2. \tag{A9}$$

[1] A. Wasiela, Y. Merle d'Aubigné, J. E. Nichols, D. E. Ashenford, and B. Lunn, Solid State Commun. **76**, 263 (1990).
[2] J. A. Gaj, W. Grieshaber, C. Bodin-Deshayes, J. Cibert, G. Feuillet, Y. Merle d'Aubigné, and A. Wasiela, Phys. Rev. B **50**, 5512 (1994).
[3] W. Grieshaber, J. Cibert, J. A. Gaj, Y. Merle d'Aubigné, and A. Wasiela, Phys. Rev. B **50**, 2011 (1994).
[4] E. L. Ivchenko, A. V. Kavokin, V. P. Kochereshko, G. R. Posina, I. N. Uraltsev, D. R. Yakovlev, R. N. Bicknell-Tassius, A. Waag, and G. Landwehr, Phys. Rev. B **46**, 7713 (1992).
[5] M. Kohl and D. D. Awschalom, J. Appl. Phys. **70**, 6377 (1991).
[6] C. Buss, R. Frey, C. Flytzanis, and J. Cibert, Solid State Commun. **94**, 543 (1995).
[7] M. Dahl, S. Gehrsitz, T. Litz, and A. Waag, in *Proceedings of XXII ICPS*, edited by D. J. Lockwood (World Scientific, Singapore, 1995), p. 2593.
[8] B. Buda, M. Dahl, N. von Truchsess, and A. Waag, J. Cryst. Growth **138**, 652 (1994).
[9] I. N. Uraltsev, E. L. Ivchenko, P. S. Kopev, V. P. Kochereshko, and D. R. Yakovlev, Phys. Status Solidi B **150**, 673 (1988).
[10] E. L. Ivchenko, V. P. Kochereshko, P. S. Kopev, V. A. Kosobukin, I. N. Uraltsev, and D. R. Yakovlev, Solid State Commun. **70**, 529 (1989).
[11] I. N. Uraltsev, V. P. Kochereshko, A. V. Kavokin, G. R. Pozina, D. R. Yakovlev, G. Landwehr, R. N. Bicknell-Tassius, and A. Waag, J. Cryst. Growth **117**, 877 (1992).
[12] K. Sato, Jpn. J. Appl. Phys. **20**, 2403 (1981).
[13] E. L. Ivchenko, Fiz. Tverd. Tela (St. Petersburg) **33**, 2388 (1991) [Sov. Phys. Solid State **33**, 1344 (1991)].
[14] L. C. Andreani and F. Bassani, Phys. Rev. B **41**, 7536 (1990).
[15] R. Kubo, J. Phys. Soc. Jpn. **12**, 1866 (1957); R. Kubo, M. Toda, and N. Hashitsume, *Statistical Physics II* (Springer-Verlag, Berlin, 1985).
[16] *Semiconductors, Physics of Group IV Elements and III–V Compounds*, edited by O. Madelung, Landolt-Börnstein, New Series, Group III, Vol. 17, Pt. b (Springer-Verlag, Berlin, 1982); *Semiconductors, Impurities and Defects in Group IV Elements and III–V Compounds*, edited by O. Madelung, Lohdolt-Börnstein, New Series, Group III, Vol. 22, Pt. a (Springer-Verlag, Berlin, 1982).
[17] Y. Merle d'Aubigné, A. Wasiela, H. Mariette, and A. Shen, in *Proceedings XXII ICPS* (Ref. 7), p. 1201.
[18] B. Leclercq, C. Rigaux, A. Mycielski, and M. Menant, Phys. Rev. B **47**, 6169 (1993).
[19] I. M. Boswarva, R. E. Howard, and A. B. Lidiard, Proc. R. Soc. London Ser. A **269**, 125 (1962).
[20] G. Dresselhaus, J. Phys. Chem. Solids **1**, 14 (1956).
[21] R. J. Elliot and R. Loudon, J. Phys. Chem. Solids **8**, 382 (1959).
[22] C. Kittel, *Quantum Theory of Solids* (Wiley, New York, 1987), p. 302.
[23] G. Bastard, *Wave Mechanics Applied to Semiconductor Heterostructures* (Les Editions de Physique, Paris, 1988).